Journal of Fluorine Chemistry 129 (2008) 662–668

Contents lists available at ScienceDirect

Journal of Fluorine Chemistry

journal homepage: www.elsevier.com/locate/fluor

Functional fluoro substituted tetrakis-metallophthalocyanines: Synthesis, spectroscopy, electrochemistry and spectroelectrochemistry

Armağan Günsel [a], Mehmet Kandaz [a,*], Atıf Koca [b], Bekir Salih [c]

[a] Department of Chemistry, Sakarya University, 54140 Esentepe, Sakarya, Turkey
[b] Chemical Engineering Department, Engineering Faculty, Marmara University, 34722 Göztepe, Istanbul, Turkey
[c] Department of Chemistry, Faculty of Science, Hacettepe University, Beytepe Campus, Ankara 06532, Turkey

ARTICLE INFO

Article history:
Received 29 February 2008
Received in revised form 21 May 2008
Accepted 21 May 2008
Available online 29 May 2008

Keywords:
Phthalocyanines
Fluorine
Electron-withdrawing
Maldi-TOF
Aggregation
Spectroelectrochemistry

ABSTRACT

In this study, electron-withdrawing fluoro-functional ligand and its tetrakis 2,9,16,23-4-(2,3,5,6-tetrafluoro)-phenoxy-phthalocyaninatometal (II) complexes, ($ZnPcOBzF_{16}$, $CuPcOBzF_{16}$ and $CoPcOBzF_{16}$) (Bz: benzene) which are organo-soluble have been prepared. Their structures were confirmed by elemental analysis, FT-IR, ^1H NMR, UV/vis and MS (Maldi-TOF) spectral data. Electron-withdrawing fluorine atoms on 2,3,5,6-position of benzene at the peripheral sites increases the solubility of the tetrakis-metallophthalocyanines. The cyclic voltammetry and differential pulsed voltammetry of the complexes show that while $CuPcOBzF_{16}$ and $ZnPcOBzF_{16}$ give ligand-based reduction and oxidation processes, $CoPcOBzF_{16}$ gives both ligand and metal-based redox processes, in harmony with the common MPc complexes. Spectroelectrochemical measurements confirm the assignments of the complexes.

© 2008 Elsevier B.V. All rights reserved.

1. Introduction

Phthalocyanines derivatives show interesting chemical and physical properties [1,2]. Therefore, excellent technologies have been developed around these functional materials in the last decade by facile substitution on the periphery (α, β, and γ) [3–6]. Due to their extended planar hydrophobic aromatic surface, phthalocyanine molecules can interact with each other by attractive π–π* stacking interactions. The interactions of phthalocyanines affect aggregation and solubility tendencies both in solution and in the solid state [7–10]. Nevertheless, it is difficult to melt and dissolve for most of them, which limits their applications in many fields [11]. The solubility of the phthalocyanines (Pcs) can be improved significantly with increasing the steric interactions in the Pc units having electron-withdrawing (–F, –Cl, –Br, $–NO_2$, etc.), and electron-donating ($–NH_2$, Ar–S–, RO–, etc.) bulky or long chain groups [11–16]. Metal phthalocyanines bearing fluorine atoms are currently receiving a great deal of attention due to their high thermal and chemical stability; they also possess interesting electron-transporting characteristics [17]. By placing stronger electron-withdrawing fluorine atoms on the Pc ring results in both the valence and conduction band energies being further lowered. Thus, $MPcF_n$ (n: number of fluorine atoms) exhibits n-type behavior, while unsubstituted phthalocyanines possess p-type due to doping with electron-accepting molecules [18]. These unusual properties of $MPcF_n$ have led scientists to expose their chemistry to use in a number of different industrial applications [19].

The goal of electrochemical study is to investigate the effect of electron-withdrawing atoms on phthalocyanine which has the potential to be an n-type Pc. It is known that the reduction and oxidation processes of the phthalocyanines are shifted to more positive potentials by the electron-withdrawing effect of these types of substituents [1].

Here, we report the synthesis and characterization of 4′-(2,3,5,6-tetrafluorophenoxy)-1,2-dicyanobenzene and its metallophthalocyanines ($ZnPcOBzF_{16}$, $CuPcOBzF_{16}$, and $CoPcOBzF_{16}$). To extend the application of the complexes we also investigate the electrochemical properties of the designed complexes.

2. Experimental

2,3,5,6-Tetrafluorophenol, diethylether, tetrahydrofuran (THF) tetrabutyl ammonium tetrafluoroborate ($TBATBF_4$), ($CuCl_2$, $Zn(O_2CMe)_2$ or $CoCl_2$) were purchased from Aldrich Chemical Co and used as received. THF was distilled from anhydrous $CaCl_2$ and

* Corresponding author. Fax: +90 264 295 59 50.
E-mail address: mkandaz@sakarya.edu.tr (M. Kandaz).

0022-1139/$ – see front matter © 2008 Elsevier B.V. All rights reserved.
doi:10.1016/j.jfluchem.2008.05.014

acetophenone. 4-Nitrophthalonitrile was prepared according to the procedure in literature [20]. Chromatography was performed with silica gel from Aldrich. All reactions were carried out under dry N_2 atmosphere. Purity of the products was tested in each step by TLC (Silica gel, $CHCl_3$, Hexane, and MeOH). FT-IR (Thin Solution Film) were recorded on ATI UNICOM-Mattson 1000 Spectrophotometer. Elemental analysis (C, H and N) was performed at the instrumental Analysis Laboratory of Marmara University. Routine UV/vis spectra were recorded on an Agillent Model 8453 diode array spectrophotometer. ^{1}H NMR and ^{13}C NMR spectra were recorded on a Bruker 300 spectrometer instruments. Multiplities are given as s (singlet), d doublet), t (triplet).

2.1. Electrochemical method

The cyclic voltammetry (CV), differential pulse voltammetry (DPV), and controlled potential coulometry (CPC) measurements were carried out with Gamry Reference 600 potentiostat/galvanostat controlled by an external PC and utilizing a three-electrode configuration at 25 °C. The working electrode was a Pt disc with a surface area of 0.071 cm^2. The surface of the working electrode was polished with a diamond suspension before each run. A Pt wire served as the counter electrode. Saturated calomel electrode (SCE) was employed as the reference electrode and separated from the bulk of the solution by a double bridge. Ferrocene was used as an internal reference. Electrochemical grade tetrabutylammonium perchlorate (TBAP) in extra pure dichloromethane (DMSO) was employed as the supporting electrolyte at a concentration of 0.10 mol dm^{-3}. High purity N_2 was used to remove dissolved O_2 at least 15 min prior to each run and to maintain a nitrogen blanket during the measurements. IR compensation was also applied to the CV scans to further minimize the potential control error.

The spectroelectrochemical measurements were carried out with an Ocean-optics QE65000 diode array spectrophotometer equipped with the potentiostat/galvanostat utilizing a three-electrode configuration of thin-layer quartz spectroelectrochemical cell at 25 °C. The working electrode was transparent Pt gauze. Pt wire counter electrode separated by a glass bridge and a SCE reference electrode separated from the bulk of the solution by a double bridge were used.

2.2. Maldi mass spectrometry

Mass spectra were acquired on a Voyager-DE^{TM} PRO Maldi-TOF mass spectrometer (Applied Biosystems, USA) equipped with a nitrogen UV-laser operating at 337 nm. Spectra were recorded both in linear and reflectron modes with average of 50 and 100 shots for linear and reflectron modes.

2.3. Maldi sample preparation

α-Cyano-4-hydroxycinnamic acid (CHCA) and dithranol (1,8-dihydroxy-10*H*-anthracen-9-one) Maldi matrix were used and prepared in chloroform at a concentration of 20 mg/mL for **2**, **3** and **4**. Maldi samples were prepared by mixing sample solutions (4 mg/mL) with the matrix solution (1:10, v/v) in a 0.5 mL eppendorf® micro tube. Finally 1 μL of this mixture was deposited on the sample plate, dried at room temperature and then analyzed. α-Cyano-4-hydroxycinnamic acid (CHCA) (20 mg/mL in acetonitrile) matrix for **4** was prepared. Maldi samples were prepared by mixing complex (2 mg/mL in acetonitrile) with the matrix solution (1:10, v/v) in a 0.5 mL eppendorf® micro tube. Finally 1 μL of this mixture was deposited on the sample plate, dried at room temperature and then analyzed like literatures [21,22].

2.4. Synthesis

2.4.1. 4-(2,3,5,6-Tetrafluorophenoxy)-1,2-dicyanobenzene (1)

2,3,5,6-Tetrafluorophenol (1.04 g, excess 10%) and 4-nitrophtlaonitrile (1.0 g, 5.78 mmol) were dissolved in dry dimethylformamide (DMF) and heated at 40 °C in N_2 atmosphere for 1 h. Then finely ground anhydrous K_2CO_3 (1.20 g; excess) was added portionwise to this mixture over 0.5 h. After the reaction mixture was stirred efficiently under N_2 for 30 h, the mixture was cooled to room temperature. Then it was poured in to ca. 200 cm^3 ice-water. The creamy precipitate thus formed was washed with water until the filtrate was clear. The crude product was dissolved in chloroform and washed with 5% $NaHCO_3$ to remove starting uncreated compounds. The creamy solution was then dried with anhydrous Na_2SO_4, and filtered. It was chromatographed over a silica gel column using a mixture of $CHCl_3$:MeOH (100/5) as eluent, giving a powder solid, 4′-(2,3,5,6-tetrafluorophenoxy)-phthalonitrile, **1**, giving a powder solid. Finally, the pure powder was dried in a vacuum. Yield: 1.28 g (75.84%); mp = 141 °C; Anal. Calcd. For $C_{14}H_4F_4N_2O$ (292 g/mol): C, 57.53; H, 1.36; N, 9.59%. Found: C, 57.15; H, 1.29; N, 9.22%. FT-IR (Thin film, disc) ν_{max} (cm^{-1}): 3083, 3052 (Ar–CH), 2236 (C≡N), 1602 (C=C), 1517 (st), 1483 (st), 1358 (C–F), 1230 (Ar–O–Ar), 935, 882, 792, 713, 505. ^{1}H NMR (DMSO-d_6) δ: 8.31 (s, H, *ortho* to Ar–C–S), 8.22 (dd, H, *ortho* to CN), 8.00 (dd, H, *meta* to CN), 6.90 (*ortho* to Ar–C–F); ^{13}C NMR ([d_6]-DMSO): δ = 163.2 (Ar–O–Ar), 149.3 (Ar–C–F), 148.8 (Ar–C–F), 147.3 (Ar–C–F), 147.3 (Ar–C–F), 140.7 (Ar–C–O), 135.2 (Ar–C– *ortho* to Ar–C–CN), 134.2 (Ar–C, *ortho* to Ar–C–CN), 131.3 (Ar–C– *ortho* to CN), 121.8 (Ar–C– *ortho* to CN), 120.0 (Ar–C– *meta* to CN) 116.1 (Ar–C– *ortho* to CN), 114.6 (Ar–CN), 101.0 (Ar–C, *ortho* to Ar–C–F), 40.8 (DMSO). EI/MS: *m*/*z* (%): 292.3 (65) [M$^+$].

2.4.2. 2,9,16,23-Tetrakis-4-(2,3,5,6-tetrafluoro)phenoxy-phthalocyaninatozinc(II) (ZnPcOBzF$_{16}$) (2)

A mixture of compound **1** (0.15 g; 0.51 mmol), anhydrous $Zn(O_2CMe)_2$ (0.04 g; 0.24 mmol), dry quinoline (∼1 cm^3), and DBU (0.05 cm^3) in a sealed tube was heated with stirring at 170–180 °C for 8 h under N_2 atmosphere. The deep green-blue product was cooled to room temperature and then the waxy solid was washed successively with MeCN and MeOH to remove any inorganic and organic impurities until the filtrate was clear. Finally the blue product was isolated by silica gel column chromatography with $CHCl_3$ and then with THF/$CHCl_3$ (1:2, v/v) as eluent and then dried in vacuo. This product is soluble in CH_2Cl_2, $CHCl_3$, DMF, DMSO and more soluble in acetone and THF.

Yield: 0.025 g (15.90%); mp > 200 °C; Anal. Calcd. For $C_{56}H_{16}F_{16}N_8O_4Zn$ (1233 g/mol): C, 54.50; H, 1.30; N, 9.08. Found: C, 54.09; H, 1.31; N, 8.78%. FT-IR (KBr thin film) ν (cm^{-1}): 3080 (w, broad, Ar–H), 1718 (vw), 1639, 1608 (C=C), 1521, 1487 (st, C–F), 1396, 1338, 1271, 1209 (Ar–S–Ar), 1122, 1019, 1068, 943 (st), 833. UV/vis ($CHCl_3$, λ_{max}/nm (log ε): 672 (4.16), 637 (1.42, agg), 608 (1.25), 346 (2.96); MS (Maldi-TOF, ditranol as matrix): *m*/*z* (100%): 1232.34 [M+H]$^+$.

2.4.3. 2,9,16,23-Tetrakis-4-(2,3,5,6-tetrafluoro)phenoxy) phthalocyaninatocopper(II) (CuPcOBzF$_{16}$) (3)

A similar preparation method used for the complex **2** was used to obtain blue-powder of **3** starting with a mixture of **1** (0.15 g; 0.50 mmol), anhydrous $CuCl_2$ (∼0.04 g; 0.24 mmol) and DBU (0.05 cm^3) in dry quinoline (∼1 cm^3). Further purification was carried out by column chromatography with silica gel (eluent: $CHCl_3$, and then THF/$CHCl_3$ (1:2, v/v)) and dried in vacuo. Complex **3** is soluble excellent in acetone, THF, soluble moderately in CH_2Cl_2 and $CHCl_3$, and slightly soluble in DMF and DMSO.

Yield: 0.020 g (12.74%); mp > 200 °C; Anal. Calcd. For $C_{56}H_{16}F_{16}N_8O_4Cu$ (1231.5 g/mol): C, 54.56; H, 1.30; N, 9.09%. Found: C, 53.95; H, 1.33; N, 8.77%. FT-IR (KBr thin film) ν_{max}/cm^{-1}: 3033 cm^{-1} (w, Ar–H, broad), 1627 (w), 1602 (C=C), 1483 (st), 1434, 1380, 1309, 1234 (st, –C–F), 1141, 1097, 964 (st), 916, 823; UV/vis (in THF), λ_{max}/nm: 670 (4.65), 636 (1.40, agg), 605 (1.25), 345 (2.72); MS (Maldi-TOF, ditranol as matrix): *m/z* (100%): 1231.23 $[M+H]^+$.

2.4.4. 2,9,16,23-Tetrakis-4-(2,3,5,6-tetrafluoro)phenoxy) phthalocyaninatocobalt(II) ($CoPcOBzF_{16}$) (4)

A similar preparation method to that used for compounds **2** and **3** was used to obtain blue-powder of **4** starting from a mixture of **1** (0.15 g; 0.5 mmol) anhydrous $CoCl_2$ (0.04 g; 0.24 mmol) and DBU (0.05 cm^3) in dry quinoline (1 cm^3). Compound **4** is soluble in CH_2Cl_2, $CHCl_3$, acetone and THF, and less soluble in DMF and DMSO. Further purification was carried out by column chromatography with silica gel (eluent: $CHCl_3$/MeOH; 10/1, and then THF) and dried in vacuo.

Yield: 0.29 g (46%); mp > 200 °C; Anal. Calcd. For $C_{56}H_{16}F_{16}N_8O_4Co$ (1227 g/mol): C, 54,77; H, 1.30; N, 9.12%. Found: C, 52.75; H, 1.31; N, 8.04%. FT-IR (KBr thin film) ν/cm^{-1}: 3074 cm^{-1} (w, Ar–H, broad), 1635 (w), 1614 (C=C), 1517 (st), 1483 (st), 1409 (st, –C–F), 1332, 1269, 1217 (Ar–S–Ar), 1173, 1093 (st), 945, 827, 748, 711; UV/vis (THF), λ_{max}/nm: 660 (4.48), 601, 339 (4.13); MS (Maldi-TOF, ACCA as matrix): *m/z* (100%): 1227.40 $[M+H]^+$.

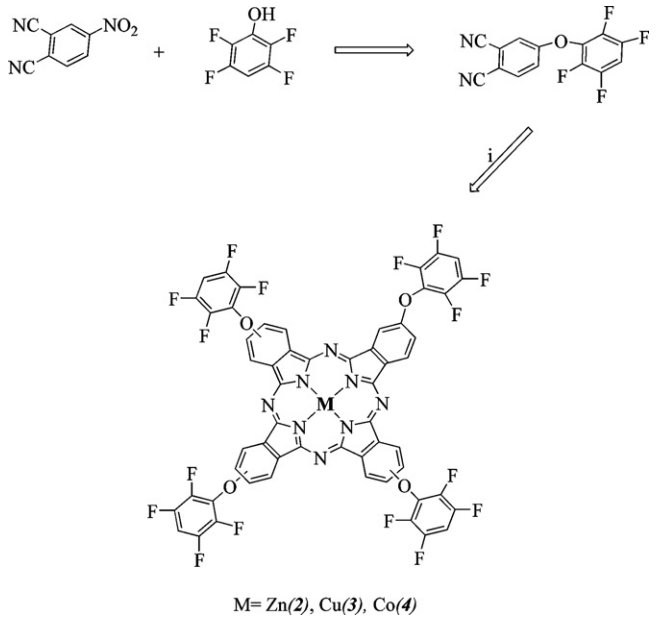

Scheme 1. Synthetic route of 4-(2,3,5,6-tetrafluorophenoxy)-1,2-dicyanobenzene and its metallo phthalocyanine (M = Zn(II) and Cu(II)). (i) 2,3,5,6-Tetrafluorophenol and 4-nitrophthalonitrile and K_2CO_3 in DMF at 40 °C for 24 h. (ii) Anhydrous $Zn(acac)_2$, and $CuCl_2$, DBU, quinoline.

3. Results and discussion

3.1. Synthesis and characterization

Novel copper, zinc and cobalt phthalocyanines (**2**, **3** and **4**) were prepared by the templated cyclization reaction from 4-(2,3,5,6-tetrafluorophenoxy)-1,2-dicyanobenzene and anhydrous $CuCl_2$, $Zn(O_2CMe)_2$ or $CoCl_2$ in the presence of high boiling quinoline solvent at 180–185 °C under N_2 atmosphere in the presence of 1,8-diazabicyclo [5.4.0] undec-7-ene (DBU) as a strong base and as shown in Scheme 1. The blue cyclotetramerization products, MPc's (M = Zn, Cu and Co) were purified by column chromatography in moderate yield (15.90% for **2**, 12.74% for **3** and 15.23 for **4**), respectively. The most obvious feature of newly synthesized phthalocyanines is their solubility in various solvents such as, benzene, chloroform, acetone and THF.

Elemental analysis results and the spectral data (^{1}H NMR, FT-IR and Maldi-TOF-MS) of the new products are consisted with the assigned formulations. The blue phthalocyanine products (M = Zn, Cu and Co) were isolated as a mixture of isomers as expected [5,21,22]. The presence of isomers could be verified with slight broadening encountered in the UV–vis absorption bands and broadening in the ^{1}H NMR when compared with those of octa-substituted phthalocyanines composed of a single isomer [5,13,15,21,22]. All the analytical and spectral data are consistent with the predicted structures. The six peripheral fluoro atoms increase the solubility of the complexes in halogenated solvents and in acetone and THF.

The FT-IR spectra were used to identify strong *–C–F* stretching band at 1480–1485 cm^{-1} on the periphery band with small shift compared to the compound **1** and strong disappearance of *–CN* band at 2236 cm^{-1} in **1** after phthalocyanine formation. Aliphatic, aromatic *–C–H*, *=C–H* peaks at above and below 3000 cm^{-1} and the rest of the spectra is closely similar to that of compound **1** and diagnosed easily.

The ^{1}H NMR spectra of **2** was almost identical with starting compound **1** except broadening and small shifts. The aromatic protons in the lower field region of the ^{1}H NMR of **1** and 14 different aromatic carbon atoms between 110 and 160 ppm in the spectrum are the most instinctive indicator signals for **1**. It is likely that the rather broad bands in the case of especially **2** were probably due to both chemical exchange associated with the aggregation–disaggregation equilibria that occurs at high concentrations used in the NMR measurements. Another reason is that the product obtained in these reactions is a mixture of four positional isomers, which are expected to show chemical shifts only slightly differing from each other [4,7–9,15,21].

Two principle π–π^* transitions are seen for Pcs: a lower energy Q band (~550–700 nm, π–π^* transition from highest occupied molecular orbital (HOMO) to lowest unoccupied molecular orbital (LUMO) of the complexes) and a higher energy B band (~300–350 nm, deeper π–π^* transition from the highest occupied MO's (a_{1u} and a_{2u}) to the LUMO (e_g)) [6]. It is known that the effect of *O*-substitution on the periphery when compared with those of *S*-substituted derivatives for all phthalocyanines was a more-shift in these intense Q bands to shorter wavelengths [5–7,11,14]. The Q band absorptions in the UV/vis absorption spectra of the phthalocyanines (**2**, **3** and **4**) were observed as single Q bands with high intensity due to a single π–π^* transition at 672, 670 and 660 nm respectively with shoulders at slightly higher energy side of the Q band for each complexes as seen in Fig. 1. The absorption positions of the synthesized compounds are dependent on the ionic radius of the metal center.

3.2. Maldi-TOF mass spectra

Positive ion Maldi-MS spectrum of **2** and **3** is given in Figs. 2 and 3. Many different Maldi matrices were tried to find intense molecular ion peak and low fragmentation under the Maldi-MS. conditions for this complex. α-Cyano-4-hydroxycinnamic acid and dithranol (1,8-dihydroxy-10*H*-anthracen-9-one) Maldi matrix yielded best Maldi-MS spectrum as seen in Figs. 2 and 3. The peak group representing the protonated molecular ion of the **2** was observed starting with 1232 Da mass and finishing 1237 Da following each other by 1 Da mass differences. This type of mass distribution results from the isotopic mass distribution of carbon

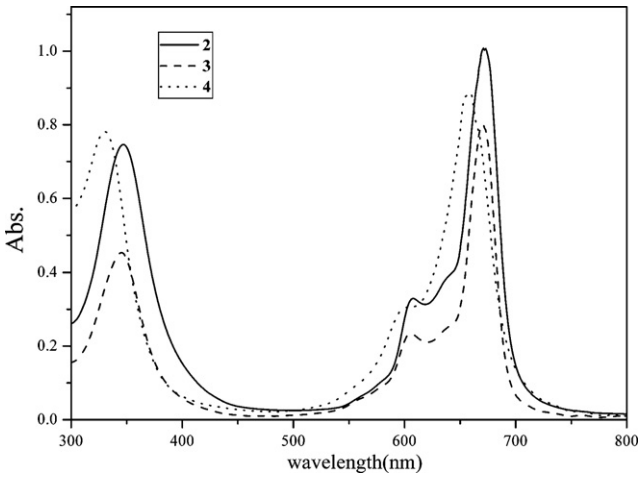

Fig. 1. UV–vis spectra of metallo phthalocyanine **2**, **3** and **4** in THF.

(mainly ^{13}C) and the isotopes of **2**. In the Maldi-MS spectrum of the **2**, beside the protonated molecular ion peak, no fragment ion was observed. This was pointed out that no leaving group was available from this complex and the complex was very stable under the Maldi matrix conditions and also under the laser energy. For the same complex very clear Maldi-MS spectrum was obtained in dithranol matrix with only protonated molecular ion peak and dithranol matrix peak. This result showed that the complex was more stable in dithranol matrix compared to the other novel Maldi matrices. Also clear Maldi spectrum showed that complex was synthesized successfully and separated efficiently. Experimental isotopic peak distributions of protonated molecular ion peak of this complex were overlapped exactly with its theoretical calculated isotopic peak distributions. Protonated molecular ion peak was observed at 1231 Da with the other isotopic peaks mainly resulted from the isotopic distribution of **3** and carbon which were exactly overlapped with the mass of the **3** calculated theoretically from the elemental composition of **3**. Beside the protonated molecular ion peak of the complex, no peak was observed between 500 and 1500 Da mass range representing the any other impurity and the fragment ions under the laser shots. Beyond the protonated molecular ion peak of the **3**, Maldi spectrum of the **3** showed very clear and no fragmentations in Maldi-MS. In the case of **3**, protonated molecular ion peak was observed at 1231 with the other three peaks following the each other by 1 Da mass difference [21,22]. For all high resolved Maldi-MS spectra of copper and zinc

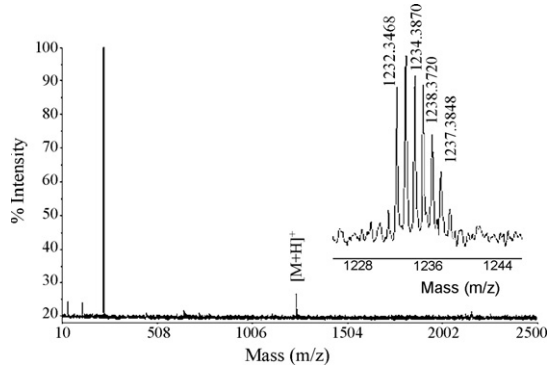

Fig. 2. Positive ion and reflectron mode Maldi-MS spectrum of **2** was obtained in dithranol (1,8-dihydroxy-10*H*-anthracen-9-one) Maldi matrix using nitrogen laser accumulating 50 laser shots. Inset spectrum shows expanded molecular mass region of the complex.

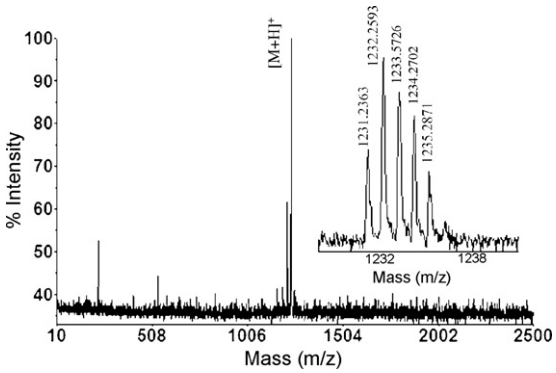

Fig. 3. Positive ion and reflectron mode Maldi-MS spectrum of **3** was obtained in dithranol (1,8-dihydroxy-10*H*-anthracen-9-one) Maldi matrix using nitrogen laser accumulating 50 laser shots. Inset spectrum shows expanded molecular mass region of the complex.

complexes, Maldi-MS spectra were obtained most efficiently using only dithranol Maldi matrix compared to the other novel Maldi matrices. Mainly protonated molecular ion peaks and the dithranol peak at around 227 Da were characterized for all copper and zinc complexes with really low intensity of the other peaks in some cases. Experimental isotopic peaks of protonated molecular ion peaks shown as inset in Maldi mass spectrum of each complex were compared the theoretical calculated isotopic peak distributions of protonated molecular ion peaks. It was concluded that all experimental isotopic peak distributions of protonated molecular ions were overlapped completely with their theoretical calculated isotopic peak distributions. These results showed that complexes were characterized precisely by Maldi-MS. All Maldi-MS results showed that dithranol was a suitable matrix for these types of metal complexes to get clearer Maldi-MS spectrum and also it could be concluded that metal complexes of these ligands were more stable in dithranol matrix. Beyond the protonated molecular ion peak of the **4**, Maldi spectrum of the **4** showed very clear and no fragmentations in Maldi-MS. In the case of **4**, protonated molecular ion peak was observed at 1227 with the other three peaks following the each other by 1 Da mass difference. This peak group is because of the isotopic distribution of cobalt and carbon in the complex structure [22]. The best Maldi-MS spectrum of this complex was obtained using α-cyano-4-hydroxycinnamic acid (ACCA) with only one fragment peak at low intensity around 1227 Da mass. If 3-indole acrylic acid (IAA) and the other conventional matrices (except ACCA) were used, more fragmentation and broad peaks could be obtained and interfering the quality of mass spectra.

3.3. Electrochemical measurements

The solution redox properties of the complexes (**2**–**4**) were studied using CV, DPV and DPSC techniques in DCM on a platinum electrode. Table 1 lists the assignments of the couples recorded and the estimated electrochemical parameters, which included the half-wave peak potentials ($E_{1/2}$), and HOMO–LUMO gaps ($\Delta E_{1/2}$). CV and DPV studies reveal that **2** (ZnPc) and **3** (CuPc) give only three reduction and two oxidation ring-based redox couples with in the potential windows of the DMSO/TBAP electrolyte and Pt electrode system. The complexes **2** and **3** give very similar voltammetric behavior accompanied by the slight potential shifts corresponding to the different metal center of the complexes (Table 1). Fig. 4 shows the CV and DPV of **2** as a representative of the complexes. For the couples II–IV, anodic to cathodic peak separations (ΔE_p) changed from ca. 60 to 150 mV with the scan rates from 10 to 500 mV s^{-1} (ΔE_p changing from 60 to 110 mV was

Table 1
Voltammetric data of the complexes with the related MPcs for comparison

Complex	Redox processes								
		I	II	III	IV	V	IV	$\Delta E_{1/2}$[a]	Ref.
2	$E_{1/2}$[b] (V *vs.* SCE)	1.08	0.68[c]	−0.80	−1.17	−2.00[c]		1.58	tw
3	$E_{1/2}$ (V *vs.* SCE)	1.05[c]	0.70	−0.75	−1.05	−1.85[c]		1.53	tw
4	$E_{1/2}$[b] (V *vs.* SCE)		0.44 (0.35)[d]	−0.42 (−0.39)[d]	−1.27	−1.65[c]	−1.95[c]	0.86	tw
CoPc[e]	$E_{1/2}$ (SCE) in THF	0.76	0.32	−0.21	−1.03	−1.25		0.53	[28]
CuPc[f]	$E_{1/2}$ (SCE) in DCM		0.15	−0.95	−1.06	−1.90		1.10	[22]
CuPc[g]	$E_{1/2}$ (Fc^+/Fc) in DCM		0.56	−0.91	−1.27			1.47	[29]
ZnPc[h]	$E_{1/2}$ (SCE) in DCM		0.85	−0.75	−1.16			1.60	[30]
CoPc[i]	$E_{1/2}$ (Ag/AgCl) in DCM	0.89	0.42	−0.40	−0.84			0.82	[31]
ZnPc[j]	$E_{1/2}$ (SCE) in DMF	1.16	0.48	−0.99				1.47	[32]

tw: this work.
[a] $\Delta E_{1/2} = E_{1/2}$ (first oxidation) − $E_{1/2}$ (first reduction) = HOMO–LUMO gap for metal-free and metallophthalocyanines having electro-inactive metal center (metal to ligand (MLCT) or ligand to metal (LMCT)) charge transfer transition gap for MPc having redox active metal center.
[b] $E_{1/2} = (E_{pa} + E_{pc})/2$ at 100 mV s^{-1} (E_{pc} for reduction, E_{pa} for oxidation for irreversible processes).
[c] Recorded by differential pulse voltammetry.
[d] E_p of the wave of aggregated species.
[e] Substituted with tetrakisdiethoxymalonyl groups.
[f] Substituted with propane 1,2-diolsulfanyl groups.
[g] Substituted with tetra(dihexoxymalonyl) groups.
[h] Substituted with tetrapentafluorobenzyloxy groups.
[i] Substituted with tetrakis (benzylmercapto) groups.
[j] Substituted with tetra-{2-(2-thienyl)}ethoxy groups.

obtained for the ferrocene reference), indicate the changing the electron transfer reactions from reversible to quasi reversible character with increasing scan rates. Reversibility is also illustrated by the similarity in the forward and reverse DPV scans (Fig. 4(dot lines)). The value of I_{pa}/I_{pc} for the couples II–IV are unity at all scan rates and the peak currents increases linearly with the square root of scan rates for scan rates ranging from 10 to 500 mV s^{-1}, suggesting purely diffusion controlled mass transfer for all couples in Fig. 4 [23–27].

The complexes **2** and **3** have both redox inactive metal centers. Therefore, in situ UV/vis spectral changes of **2** are given as a representative of the spectral chances of MPc having redox inactive metal center. As shown in Fig. 5A, there are two distinct spectroscopic changes are recorded during the potential application at the first reduction process of the complex **2**. First of all, while the intensity of Q band at 680 nm do not change, the band at 630 nm assigned to the aggregated species decrease in intensity (inset in Fig. 5A). These changes support the aggregation–disaggregation equilibrium of **2**. Then as shown in Fig. 5A, while the intensity of Q band at 680 nm decreases without shift, two new bands in the MLCT regions at 450, and 576 nm are recorded. Change in the intensity of the Q band without shift and observation

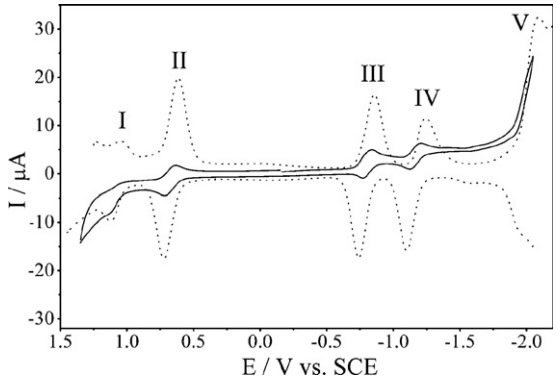

Fig. 4. CVs (solid lines) and DPVs (dot lines) of **2** (5.0×10^{-4} mol dm^{-3}). For CV, scan rate: 0.100 mV s^{-1}. For DPV, pulse width: 50 ms; pulse height: 100 mV; step height: 5 mV; step time: 100 mV; scan rate: 50 mV s^{-1}.

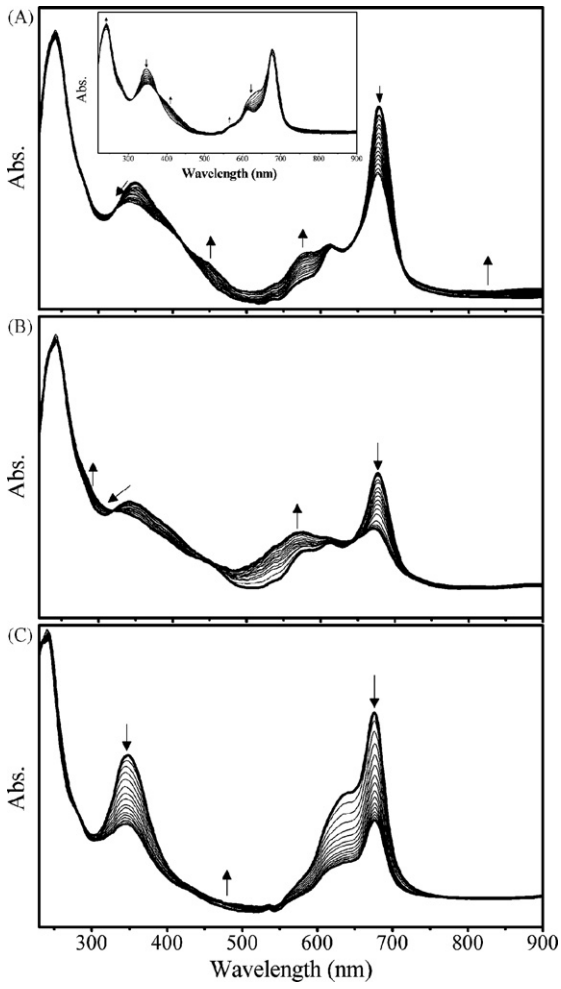

Fig. 5. In situ UV/vis spectral changes of **2**. (A) $E_{app} = -0.90$ V. (B) $E_{app} = -1.20$ V. (C) $E_{app} = 0.75$ V.

of the new bands in the MLCT regions are characteristics of ring-based processes [23,27–35]. Color change from green to blue support the generation of monoanionic [Zn (II) Pc $(-3)]^{-1}$ species during the process. The process has isosbestic points at 321, 411, 641, and 714 nm in the spectra. Further reduction of the monoanionic [Zn(II)Pc$(-3)]^{-1}$ species causes to decrease in the intensity of the Q band and increase in the intensity of the band at 576 nm (Fig. 5B). B band shift from 342 to 330 nm by decreasing at the same time during this process. The process has isosbestic points at 320, 452, and 640 nm in the spectra. These spectroscopic changes are assigned to the process, [Zn(II)Pc$(-3)]^{-1}$/ [Zn(II)Pc$(-4)]^{-2}$. Color change from blue to light purple support the generation of dianionic [Zn(II)Pc$(-4)]^{-2}$ species during the process. Fig. 5C shows the ligand-based oxidation processes of the complex under 0.75 V potential application. Surprisingly all bands decrease in intensity during this process, while the intensity of the region at around 480 nm increase slightly. The process has isosbestic points at 278, 433 and 534 nm in the spectra. These spectroscopic changes indicate the formation of the [Zn(II)Pc$(-1)]^{+}$ species, and then decomposition of the [Zn(II)Pc$(-1)]^{+}$ species during the 0.75 V potential application [23,30–35].

The complex **4** give four one-electron reduction processes labelled as III at −0.42 V (III′ at −0.39 V), IV at −1.27 V, at −1.65 V and −1.95 V and a one-electron oxidation processes labelled as II at 0.85 V (II′ at 1.25 V) *vs.* SCE at 0.100 V s^{-1} scan rate (Fig. 6). The assignments of the redox couples are confirmed below using spectroelectrochemistry measurements. As shown in Fig. 6, the first reduction and oxidation couples are split into two peaks. This behavior is due to the aggregation of the complex in solution. Dilution of the solution changes the aggregation–disaggregation equilibria of the complex. While the solution is diluted, peak current of the wave III′ assigned to the aggregated species gets smaller much more than that of III, however it is present even in very diluted solution [1,24,25].

Spectroelectrochemical measurements (SE) were used to confirm some of the assignments of the complex **4** in the CVs. The experiments were performed using optically transparent thin-layer quartz electrochemical cell. Fig. 7A shows the in situ UV–vis spectral changes during the controlled potential reduction of **4** at −0.50 V *vs.* SCE corresponding to the redox process labeled III and III′ in the CV (Fig. 6). While the intensity of the absorption of the Q band corresponding to the neutral [Co(II)Pc(−2)] species decreases at 659 nm, a new Q band corresponding to the electro-generated reduced [Co(I)Pc$(-2)]^{-1}$ species at 704 nm appears. At the same time a split bands at 434 and 470 nm grows, while the B band increases slightly in intensity with a blue shift from 330 to 317 nm during this process. Moreover, broadness of the Q band due to the aggregation decreases during this potential application by decrease of the adsorption at around 630 nm. The spectral changes

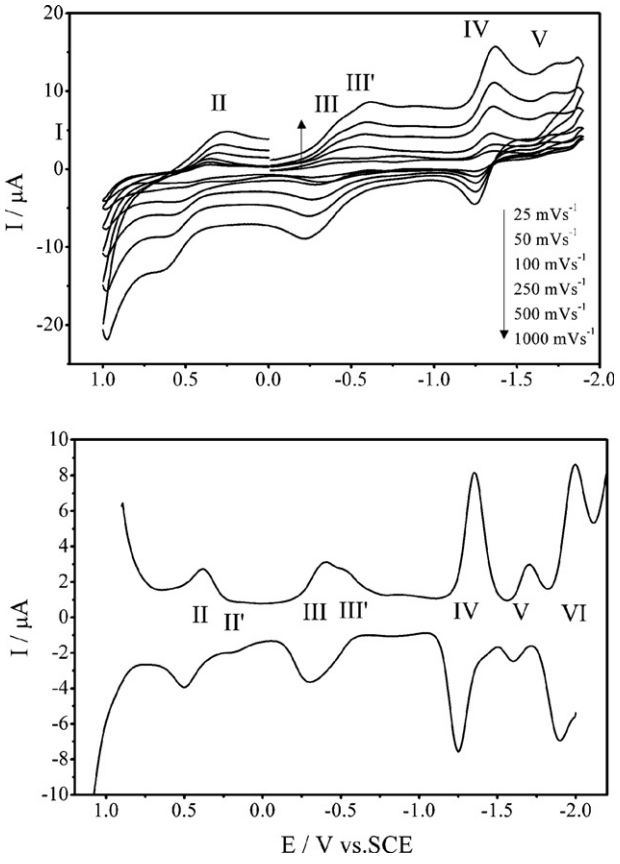

Fig. 6. CVs and DPVs of **4** (5.0×10^{-4} mol dm^{-3}) at various scan rates (for DPV, pulse width: 50 ms; pulse height: 100 mV; step height: 5 mV; step time: 100 mV; scan rate: 50 mV s^{-1}).

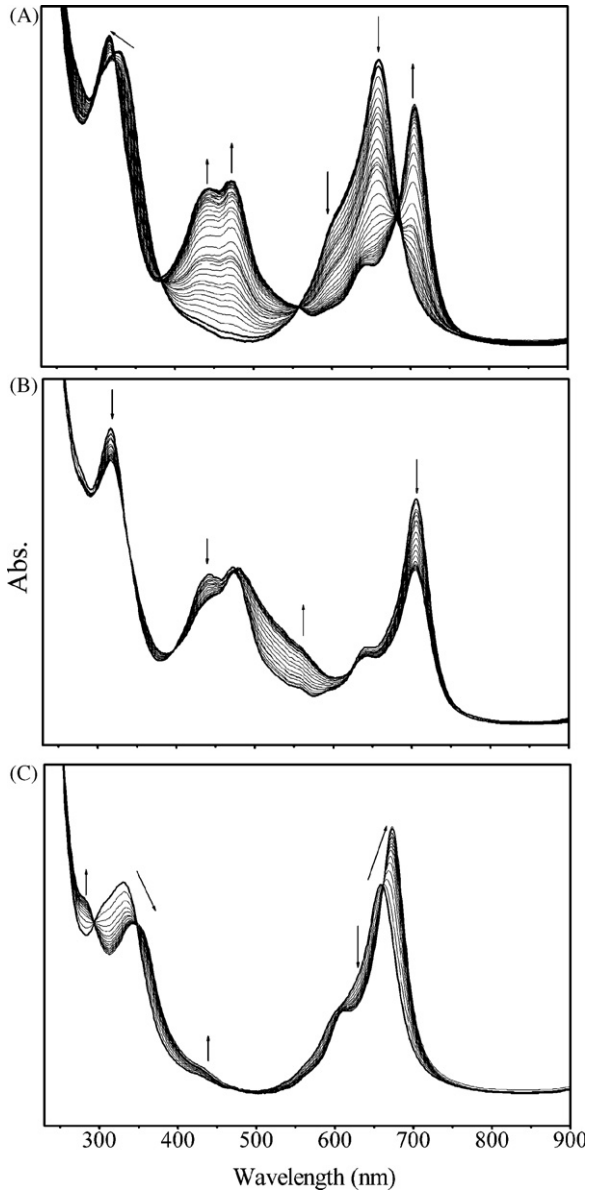

Fig. 7. In situ UV–vis spectral changes of **4**. (A) E_{app} = −0.50 V. (B) E_{app} = −1.35 V. (C) E_{app} = 0.60 V.

in Fig. 7A are typical of metal-based reduction in phthalocyanine complexes. The shift of the Q band from 659 to 704 nm and observation of new bands at 434 and 370 nm (MLCT) are characteristic of metal-based processes [23,31–35]. Observation of a split band between 400–500 nm and decrease of the Q band broadness shows the aggregation desegregation equilibria present in solution. As shown in Fig. 7A, the process at −0.50 V potential applications occurred with clear isosbestic points at 290, 380, 556 and 686 nm in the spectra. The color of the solution is changed from blue to green during the process. Change to the original spectrum and color after the potential application at 0.00 V indicates the reversibility of the process. During the controlled potential reduction of **4** at −1.35 V *vs.* SCE corresponding to the redox process labeled IV (Fig. 7B), the absorptions of the Q bands at 704 nm decreases in intensity without shift, while one of the split bands at 495 nm increase in intensity. At the same time a broad band increases at around 550 nm while the B band at 317 nm decreases in intensity. The color of the solution is changed from green to red during the process. Change to the original spectrum and color after the potential application at −0.50 V indicates the reversibility of the process. The process at −1.35 V *vs.* SCE potential application has isosbestic points at 336, 393, 476 and 625 nm in the spectra. The spectral changes in Fig. 7B are typical of ligand-based reduction assigned to $[Co(I)Pc(-2)]^{-1}/[Co(I)Pc(-3)]^{-2}$ redox process [23,31–35]. On potential application at 0.60 V, the intensities of the Q bands increases with a red shift from 658 to 674 nm, while the broadness of the Q band gets sharper by decrease of the absorption at around 600 nm (Fig. 7C). At the same time while the B band shifts from 330 to 344 with decreasing, a new band appears at 284 nm. The spectral changes in Fig. 7C, especially shifting of the Q band with increasing are typical of metal-based oxidation in phthalocyanine complexes and the process is easily assigned to $[Co(II)Pc(-2)]/[Co(III)Pc(-2)]^{+1}$ redox process [23,31–35]. The process has isosbestic points at 293, 347, 484, and 662 nm in the spectra and blue to green color changes upon the potential application at 0.60 V. Obtaining the original color and spectrum after the potential application at 0.0 V shows the reversibility of the process. During CPC studies, complete electrolysis of the solution of the complexes at the end of the solvent windows was achieved, and the time integration of the electrolysis current was recorded. The CPC studies indicated that the number of electrons transferred for each of the couples was found to be approximately one.

As a result, the effects of peripheral fluoro atoms and metal ions on the electronic structure of metal (II) phthalocyanines, ($ZnPcOBzF_{16}$, $CuPcOBzF_{16}$ and $CoPcOBzF_{16}$), which are exhibited interesting solubility have been investigated. It is important to mention here that for high-technological applications the solubility of phthalocyanines is important. Phthalocyanines synthesized are soluble considerably in weak and medium polar solvents, such as benzene, CH_2Cl_2, $CHCl_3$, acetone and THF. Complex **3** ($CuPcOBzF_{16}$) has showed less solubility than the others in strongly polar solvents such as DMF and DMSO due to aggregation phenomena, even if they have the same peripheral structure [1]. The solubility of MPcs is also affected by the atomic radius of central metal ions and by the peripheral substituents. The blue shift of the complexes compared to the parent phthalocyanine was due to fluorine group at the peripheral substituents. However, stronger electron-withdrawing fluorine atoms on the Pc ring also affect the electrochemical behavior of the complexes. The approach described here may be useful for fabrication of the highly soluble semiconductor phthalocyanine devices whose conducting properties will be the subject of our future interest.

Acknowledgements

We thank the Research Funds of Sakarya University, State Planning Organization (DPT-2004 P.No.: 2003K120970) and TÜBİTAK (P.No.: TBAG 108T094; MAG-106M286).

References

[1] C.C. Leznoff, A.B.P. Lever, in: C.C. Leznoff, A.B.P. Lever (Eds.), Phthalocyanines: Properties and Applications, vol. 1–4, VCH, Weinheim, 1989–1996.
[2] J. Jiang, K. Kasuga, D.P. Arnold, in: H.S. Nalwa (Ed.), Supramolecular Photosensitive and Electroactive Materials, Academic Press, San Diego, CA, 2001 , pp. 188–189 (and references therein).
[3] M. Calvete, G.Y. Yang, M. Hanack, Synth. Met. 141 (2004) 231–243.
[4] M. Kandaz, S.L.J. Michel, B.M. Hoffman, J. Porphyr. Phthalocya. 7 (2003) 700–712.
[5] P. Tau, T. Nyokong, Polyhedron 25 (2006) 1802–1810.
[6] J.J. Simon, H.J. Andre, Molecular Semiconductors, Springer, Berlin, 1985.
[7] M. Kandaz, I. Yılmaz, Ö. Bekaroğlu, Polyhedron 19 (2000) 1802–1810.
[8] M.J. Cook, J. Mater. Chem. 6 (1996) 677.
[9] M. Kandaz, H.S. Çetin, A. Koca, A.R. Özkaya, Dyes Pigments 74 (2) (2007) 298–305.
[10] S.L.J. Michel, A.G.M. Barrett, B.M. Hoffman, Inorg. Chem. 42 (2003) 814.
[11] Z. Odabaş, A. Altındal, A.R. Özkaya, M. Bulut, B. Salih, Ö. Bekaroğlu, Polyhedron 26 (2007) 3505–3512.
[12] M. Matsuoka, Infrared Absorbing Dyes, Plenum Press, New York, 1990.
[13] M. Kandaz, Ö. Bekaroğlu, Chem. Ber. 135 (1997) 1833–1836.
[14] M. Özer, A. Altındal, A.R. Özkaya, M. Bulut, B. Salih, Ö. Bekaroğlu, Polyhedron 25 (2006) 3593–3602.
[15] M. Kandaz, M.N. Yaraşır, A. Koca, Ö. Bekaroğlu, Polyhedron 21 (2002) 255–263.
[16] M. Kandaz, Ö. Bekaroğlu, J. Porphyr. Phthalocya. 3 (1999) 339–345.
[17] B.A. Bench, W.W. Brennessel, H.-J. Lee, S.M. Gorun, Angew. Chem. Int. Ed. 41 (5) (2002) 750–754.
[18] Y. Liu, D. Yang, C. Wang, J. Phys. Chem. B 110 (2006) 20789–20793.
[19] T. Manaka, M. Iwamoto, Thin Solid Films 438/439 (2003) 157–161.
[20] J.G. Young, W. Onyebuagu, J. Org. Chem. 55 (1990) 2155–2159.
[21] M.N. Yaraşır, M. Kandaz, A. Koca, B. Salih, Polyhedron 26 (5) (2007) 1139–1147.
[22] M. Kandaz, A.R. Özkaya, A. Koca, B. Salih, Dyes Pigments 74 (2) (2007) 483–489.
[23] K. Hesse, D. Schlettwein, J. Electroanal. Chem. 476 (1999) 148–158.
[24] A.B.P. Lever, S.R. Pickens, P.C. Minor, S. Licoccia, B.S. Ramaswany, K. Magnell, J. Am. Chem. Soc. 103 (1981) 6800–6806.
[25] R. Li, X. Zhang, I.P. Zhu, D.K.P. Ng, N. Kobayashi, J. Jiang, Inorg. Chem. 45 (2006) 232.
[26] P.T. Kissinger, W.R. Heineman, Laboratory Techniques in Electroanalytical Chemistry, 2nd ed., Marcel Dekker, New York, 1996.
[27] A.J. Bard, L.R. Faulkner, Electrochemical Methods: Fundamentals and Applications, 2nd ed., Wiley, New York, 2001.
[28] A. Koca, H.A. Dinçer, M.B. Koçak, A. Gül, Russ. J. Electrochem. 42 (2006) 31–37.
[29] M.K. Şener, A. Koca, A. Gül, M.B. Koçak, Polyhedron 26 (2007) 1070–1076.
[30] A. Koca, A.R. Özkaya, M. Selçukoğlu, E. Hamuryudan, Electrochim. Acta 52 (2007) 2683–2690.
[31] B. Agboola, K.I. Ozoemena, T. Nyokong, Electrochim. Acta 51 (2006) 4379.
[32] J. Obirai, T. Nyokong, Electrochim. Acta 50 (2005) 5427–5434.
[33] Y.H. Tse, A. Goel, M. Hu, C.C. Leznoff, J.E. Van Lier, A.B.P. Lever, Can. J. Chem. 71 (1993) 742–753.
[34] P. Matlaba, T. Nyokong, Polyhedron 21 (2002) 2463–2472.
[35] A. Koca, A.R. Özkaya, Y. Arslanoğlu, E. Hamuryudan, Electrochim. Acta 52 (2007) 3216–3221.